Atmospheric Research 98 (2010) 57–68

Contents lists available at ScienceDirect

Atmospheric Research

journal homepage: www.elsevier.com/locate/atmos

On characterizing the error in a remotely sensed liquid water content profile

Kerstin Ebell [a,*], Ulrich Löhnert [a], Susanne Crewell [a], David D. Turner [b]

[a] Institute for Geophysics and Meteorology, University of Cologne, Cologne, Germany
[b] University of Wisconsin-Madison, Madison, Wisconsin, USA

ARTICLE INFO

Article history:
Received 15 September 2009
Received in revised form 7 May 2010
Accepted 1 June 2010

Keywords:
Liquid water content
Retrieval
Sensor synergy
Information content
Remote sensing of clouds

ABSTRACT

The accuracy of a liquid water content profile retrieval using microwave radiometer brightness temperatures and/or cloud radar reflectivities is investigated for two realistic cloud profiles. The interplay of the errors of the a priori profile, measurements and forward model on the retrieved liquid water content error and on the information content of the measurements is analyzed in detail. It is shown that the inclusion of the microwave radiometer observations in the liquid water content retrieval increases the number of degrees of freedom (independent pieces of information) by about 1 compared to a retrieval using data from the cloud radar alone. Assuming realistic measurement and forward model errors, it is further demonstrated, that the error in the retrieved liquid water content is 60% or larger, if no a priori information is available, and that a priori information is essential for better accuracy. However, there are few observational datasets available to construct accurate a priori profiles of liquid water content, and thus more observational data are needed to improve the knowledge of the a priori profile and consequentially the corresponding error covariance matrix. Accurate liquid water content profiles are essential for cloud-radiation interaction studies. For the two cloud profiles of this study, the impact of a 30% liquid water content error on the shortwave and longwave surface fluxes and on the atmospheric heating rates is illustrated.

1. Introduction

Clouds are the most significant modulator of the surface radiation budget and strongly affect the vertical redistribution of energy in the atmosphere, which may influence the cloud structure itself, but also the large-scale dynamics (Wang and Rossow, 1998). In the last decade several studies focused on the characterization of long-term cloud properties and their associated effects on radiative fluxes and heating rates (e.g. Mace et al., 2006a; Mace et al., 2006b; Mace and Benson, 2008; Mather et al., 2007; McFarlane et al., 2008). In order to assess these effects, the cloud macrophysical and microphysical properties, including the liquid water content (LWC) profile, must be accurately described. However, in-situ measurements of LWC are only available for certain campaigns (e.g. Korolev et al., 2007) and are therefore strongly limited in space and time. Thus, other retrieval techniques, which include, for example, cloud radar information, have to be applied to retrieve long-term data sets of cloud liquid water profiles. Such data sets are not only desirable for cloud-radiation interaction studies but also for the development of parameterizations for cloud microphysical processes and for the evaluation of cloud liquid water profiles in numerical weather prediction (NWP) and climate models. Due to the lack of observations, the evaluation of this prognostic model variable is rather difficult compared to other model variables.

In order to retrieve vertical information on cloud water, the vertical profile of cloud radar reflectivity is commonly used (e.g. Mace et al., 2006a; Mather et al., 2007; McFarlane et al., 2008). Since the radar reflectivity and the liquid water content are both functions of the cloud droplet spectrum, attempts have been made to relate the radar reflectivity Z, i.e. the sixth moment of the drop size distribution, with the liquid water content, i.e. the third moment (Atlas 1954; Sauvageot and Omar 1987; Fox and Illingworth 1997). The cloud droplet

* Corresponding author. Tel.: +49 221 4701777; fax: +49 221 4705161.
E-mail address: kebell@meteo.uni-koeln.de (K. Ebell).

0169-8095/$ – see front matter © 2010 Elsevier B.V. All rights reserved.
doi:10.1016/j.atmosres.2010.06.002

spectrum results from a number of complex processes (e.g. nucleation, diffusion, collision and coalescence) and is therefore highly variable even within a cloud (Khain et al., 2008). As a result, no unique Z-LWC relation exists. If a few drizzle drops are present in a cloud, they dominate the reflectivity, but contribute negligibly to the LWC. This effect leads to large errors in the derived LWC values (see, for example, Fig. 2 in Löhnert et al., 2008) and the empirical relationships fail.

To better constrain LWC profiles, passive atmospheric emission measurements in the microwave region can be used. Although microwave radiometer (MWR) observations alone show only little skill in determining the vertical distribution of cloud liquid water (Crewell et al., 2009), they are very well suited to derive the vertically integrated liquid water content, the liquid water path (LWP; e.g., Westwater, 1978). In the microwave regime, the cloud emission is proportional to the frequency squared and the cloud contribution to the signal strongly increases with frequency. Two-channel microwave radiometers usually measure at one frequency in the window region where liquid water dominates the emission (e.g., between 30 and 36 GHz) and at another one on the wing of a water vapor absorption line (e.g., 24 GHz). The latter channel is used to correct for the influence of the water vapor in the LWP retrieval. The accuracy of such dual-channel retrievals is typically about 25–30 gm^{-2} (Turner et al., 2007a). The uncertainty can be improved by including additional frequencies in the retrieval, for example the 90 or 150 GHz channel, which are both very sensitive towards liquid water. Crewell and Löhnert (2003) have shown, for example, that the inclusion of the 90 GHz channel leads to an accuracy in LWP of better than 15 gm^{-2}. In order to further decrease the uncertainty of LWP in cases where LWP is low ($<100\ gm^{-2}$), Turner (2007) followed a sensor synergy approach combining MWR and spectral infrared data. He showed that the random error for LWP using this synergetic approach is less than 4% in cases with $LWP<50\ gm^{-2}$.

The need for *sensor synergy*, i.e. the combination of information from different active and passive remote sensing instruments, to derive cloud macrophysical (e.g. Wang and Sassen, 2001; Illingworth et al., 2007) and microphysical properties (e.g. Frisch et al., 1998; Löhnert et al., 2004) has been identified in the past. For example, Frisch et al. (1998) derived profiles of LWC by taking the LWP of the MWR and applying the normalized square root of the radar reflectivity as a vertical weighting function. Löhnert et al. (2004, 2008) took a step forward and integrated ground-based microwave radiometer, cloud radar and a priori information, e.g. from radiosondes, in the framework of the *optimal estimation equations* (e.g. Rodgers, 2000). This so-called Integrated Profiling Technique (IPT) has been successfully used to derive profiles of temperature, humidity and liquid water content and corresponding error estimates. The resulting cloud water profiles are not only consistent with respect to the cloud radar measurements but also to the MWR brightness temperatures (TBs).

Generally, deriving such profiles directly from the measurements is an ill-conditioned problem, because many solutions fit the data and small errors in the measurements may have a large effect on the derived atmospheric profiles. Thus, it is indispensable to include additional information, namely *a priori data*, in the retrieval to constrain the solution space. For temperature and humidity profiles, radiosonde data can be used in this respect, since radiosondes directly provide profile information on these variables. For LWC, the provision of an a priori profile is a more demanding task, since, as mentioned previously, in-situ measurements are strongly limited in space and time. Thus, this information has to be obtained from the output of NWP models or from simple cloud models (e.g., Karstens et al., 1994; Salonen and Uppala, 1991; Mattioli et al., 2006), which diagnose the LWC from the humidity profiles measured during radiosonde ascents. These cloud models first detect the cloud boundaries by threshold values in the relative humidity and subsequently calculate the LWC as a function of height above the cloud base. In the cloud model by Karstens et al. (1994), for example, the adiabatic LWC is calculated first and then corrected for effects of dry entrainment, freezing drops, and precipitation using an empirical relationship by Warner (1955). Usually, these models are tuned to fit observed MWR brightness temperatures (e.g. Mattioli et al., 2006). However, the accuracy of the LWC determined by the cloud models is not well known and a derivation of a quantitative error estimate is in general difficult.

In this study, we want to analyze the *interplay of the errors* of the a priori profile, measurements and forward model in the LWC retrieval and the associated effect on the *retrieved LWC error* and on the *information content* of the measurements. Given realistic error estimates for the measurements and the forward model, the accuracy of the a priori profile required for a reasonable LWC error is assessed. Furthermore, the information content of different measurement combinations with respect to the derivation of cloud liquid water profiles is investigated. The measurements encompass microwave radiometer brightness temperatures and/or cloud radar reflectivities depending on the chosen configuration of the experiment. By means of two typical cloud cases, the *benefit of the synergy* of MWR and cloud radar is demonstrated. Thus, this work is a follow-up of the study by Crewell et al. (2009), who focused on the LWC retrieval using MWR measurements alone. In the next section, we introduce the two cloud cases and the analysis method used, followed by a comprehensive evaluation of the information content and the retrieved LWC error given different measurement combinations and error assumptions (Section 3).

2. Methodology

For this analysis, we have selected two single-layer liquid cloud cases (Fig. 1) observed at the Atmospheric Radiation Measurement programs Mobile Facility (AMF) site in the Black Forest, Germany. Both profiles are solutions of the IPT, which has been applied to the whole data set of the nine-month AMF measurement period, from April to December 2007. Information on the occurrence and vertical location of clouds is included in the retrieval by means of the Cloudnet Target Categorization product (Illingworth et al., 2007), which is itself a synergy product of cloud radar, ceilometer, microwave radiometer and model data. Once the position and extension of a cloud are known, microwave radiometer, cloud radar and radiosonde information are integrated via the

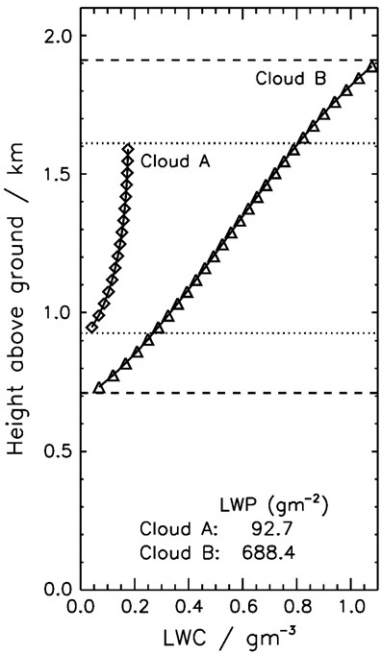

Fig. 1. LWC profiles of two water clouds without drizzle on 8 Sep 2007 at 14:19 UTC (cloud A) and on 12 Sep 2007 at 10:50 UTC (cloud B) at the AMF site in the Black Forest, Germany. Cloud boundaries have been determined from the Cloudnet Target Categorization product. The LWC profiles have been retrieved by combining a priori, cloud radar and microwave radiometer information in the framework of an optimal estimation technique.

optimal estimation technique to retrieve profiles of LWC, as well as temperature and humidity profiles. The LWC profiles are defined on the AMF cloud radar height grid that has a spatial resolution of about 43 m. The selected profiles represent a cloud with a LWP of about 90 gm^{-2} (case A) and a thickness of about 640 m, or 16 cloud radar levels, and a thick cloud (case B) having a LWP of about 690 gm^{-2} and a thickness of about 1160 m, or 28 cloud radar levels (Fig. 1). Crewell et al. (2009) have shown that the median LWP and thickness of a single-layer water cloud for the AMF site in the Black Forest is about 80 gm^{-2} and 300 m, respectively (Table 1 in Crewell et al., 2009). With regard to LWP, cloud A represents a common cloud, whereby its vertical extension is rather thick compared to the average value. However, about 50% of all single-layer water clouds have a cloud thickness between 300 and 700 m at this AMF site. Note that the IPT-retrieved profiles must not be interpreted as an explicit solution of the inverse problem but as the most probable solution of a Gaussian-distributed probability density function. Thus, both profiles describe a realistic vertical distribution of cloud liquid water.

On the basis of these two profiles, we perform our analysis employing optimal estimation theory (Rodgers, 2000). This formalism allows for a detailed analysis of the retrieved LWC error and of the information content of a set of observations. For this purpose, the covariance matrix $\mathbf{S}_a$ of the a priori LWC profile, the error covariance matrix of the observations $\mathbf{S}_e$, and the Jacobian of the forward model **F** for microwave and radar observations with respect to the LWC profile **K** have to be defined. The Jacobian **K** is given by $\mathbf{K}=\partial\mathbf{F}(\mathbf{x})/\partial\mathbf{x}=\partial\mathbf{y}/\partial\mathbf{x}$, with $\mathbf{x}=\log_{10}(\mathbf{LWC})$ and $\mathbf{y}=(\mathbf{Z},\mathbf{TB})$. The optimal estimation approach assumes that the retrieved parameters are Gaussian-distributed. Since this is not valid for the LWC, we consider log(LWC) instead, which more closely conforms to a Gaussian distribution. The measurement vector **y** encompasses the cloud radar reflectivity at 95 GHz and MWR brightness temperatures in the K-band (22–32 GHz, 7 channels) and in the V-band (51–59 GHz, 7 channels) as well as at 90 and 150 GHz. The K-band and the K-band plus V-band frequencies are typical for a dual frequency MWR and for a standard MWR profiler, respectively. For the theoretical studies presented here, only the measurement errors have to be known rather than the measurements themselves.

The error covariance of the optimal solution **S** can be calculated by

$$\mathbf{S} = \left(\mathbf{K}^T\mathbf{S}_e^{-1}\,\mathbf{K} + \mathbf{S}_a^{-1}\right)^{-1} \quad (1)$$

The diagonal elements of **S** give an estimate of the mean quadratic error of the LWC. The off-diagonal components describe the correlation of the retrieved LWC errors at different heights.

A measure for the information content of an observation in the retrieved profile is the number of *degrees of freedom for signal* (DGF) which provides the number of independent pieces of information that are determined from the measurement. In this context, the averaging kernel matrix **A** has to be calculated, which describes the sensitivity of the retrieved profile to the true state, i.e. $\mathbf{A}=\delta\ \log(\mathrm{LWC}_{\mathrm{retrieved}})/\delta\ \log(\mathrm{LWC}_{\mathrm{true}})$. The averaging kernel matrix can be determined from the optimal estimation equations as

$$\mathbf{A} = \mathbf{S}\cdot\left(\mathbf{K}^T\mathbf{S}_e^{-1}\,\mathbf{K}\right). \quad (2)$$

The number of degrees of freedom for signal is given by the trace of **A**.

If not explicitly mentioned, $\mathbf{S}_e$ and $\mathbf{S}_a$ are set to diagonal matrices in this analysis. This means that we assume the measurement and forward model errors encapsulated by $\mathbf{S}_e$, as well as the errors of the a priori profile in $\mathbf{S}_a$, to be uncorrelated (the effect of correlated errors are discussed in Sections 3.3 and 3.4). For the brightness temperatures, a random error of 0.5 K is applied, which is on the order of magnitude of the measurement noise (Rose et al., 2005). For the radar reflectivities, a random error of 3 dB is assumed, which is a reasonable estimate for the calibration error of most cloud radar systems. In particular, intercomparison measurements of the AMF cloud radar and the collocated 35.5 GHz MIRA36-S cloud radar revealed differences in the radar reflectivities of 3 dB (Handwerker and Miller, 2008). Systematic errors cannot be included in $\mathbf{S}_e$, which may lead to bias errors in the retrieval solution. In case of the TBs, systematic errors in the forward model may be related, for example, to inaccurate humidity and temperature profiles or to uncertainties in the absorption model (see discussion below).

The MWR measurements and the LWC profiles are related by a forward model, which is a microwave radiative transfer operator for nonscattering cases. Absorption due to water vapor and oxygen are calculated by the Rosenkranz absorption model (Rosenkranz, 1998), and absorption due to liquid

water is computed according to Liebe et al. (1991). It is difficult to estimate the error of the Rosenkranz model itself. Differences in simulated and observed brightness temperatures may not only be attributed to deficiencies in the radiative transfer model but also to inaccurate input and measurement data. However, Turner et al. (2009) applied carefully checked, cloud-free radiosonde data to different microwave radiative transfer models and compared the computed brightness temperatures at 150 and 31.4 GHz to independent measurements of two collocated MWRs. Both MWR showed an excellent agreement at 150 GHz with a bias of −0.12 K and a root mean square difference of 1.29 K. In case of the Rosenkranz model, the comparison between simulated and observed brightness temperatures at 150 (31.4) GHz revealed a bias and a root mean square error of 0.74 (−0.08) K and 2.52 (0.28) K, respectively. Compared to other models, e.g. Liebe et al. (1993) and Clough et al. (2005), these differences are relatively small. However, the forward model uncertainty may be larger than the measurement error itself and generally cannot be neglected.

In order to model the radar reflectivities, we use the relation by Fox and Illingworth (1997) for a cloud without drizzle, which has the form $Z = a * LWC^b$, with the parameters $a = 0.012$ and $b = 1.6$. Krasnov and Russchenberg (2002, 2006) applied this Z-LWC relation to in situ aircraft measurements and estimated the error of the forward model to be 1.5 to 3 dB. In drizzle situations, Z-LWC relationships are considerably less accurate and the forward model error becomes substantially larger than the measurement error. However, we start with an overall error of 0.5 K and 3 dB for the brightness temperatures and the radar reflectivities, respectively, keeping in mind that the error may be considerably larger due to forward model uncertainties. The effect of larger errors in $\mathbf{S}_e$ on the retrieved error and the information content will be investigated in Section 3.2 and 3.5.

3. Information content and error estimates

Given the diagonal matrices $\mathbf{S}_a$ and $\mathbf{S}_e$ as defined in Section 2, we calculated corresponding error estimates according to Eq. (1) for the profiles in Fig. 1 (see example for one experiment configuration in Fig. 2). Since we derive log(LWC), errors in LWC are not symmetric. For the following analysis we computed a mean error of the profile by calculating a mean relative error for each height and by averaging these errors over all height levels.

In order to characterize the influence of the a priori LWC profile on the retrieved LWC error and on the DGF, the uncertainty in the a priori profile is increased step-wise from $6 \cdot 10^{-4}$ gm^{-3} (0.2% rel. error) to 7 gm^{-3} (2733% rel. error) for a fixed set of observations. A small uncertainty implies that the a priori profile has a large weight in the solution. If the uncertainty of the a priori LWC profile increases, the influence of the a priori profile in the LWC retrieval decreases and more weight is put on the measurements. This variation of the a priori uncertainty has an effect on the DGF as well as on the retrieved LWC error. As an example, Fig. 3 shows the impact of the a priori uncertainty on the DGF and on the retrieved LWC error for a retrieval including only the K-band measurements of the MWR. In Fig. 3a, the DGF and the retrieved LWC errors are shown *as a function of the a priori uncertainty*. For a better comparison to Fig. 3a, the chosen a priori errors are plotted against the retrieved LWC errors in Fig. 3b. Note, however, that the retrieved error is a function of the a priori error, and not vice versa.

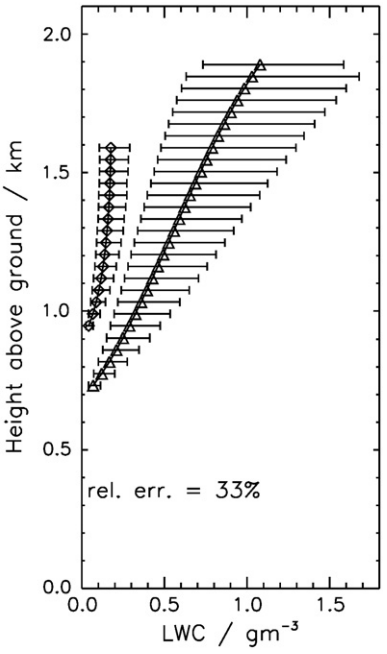

Fig. 2. Example for the retrieved errors of the LWC profiles in Fig. 1. A TB error of 0.5 K and an a priori uncertainty of $\log(LWC/gm^{-3}) = 0.175$ (corresponding to a relative a priori uncertainty of 34%) is assumed. In this example, the retrieval includes the MWR brightness temperatures of the K-band only.

Increasing the magnitude of the diagonal elements in $\mathbf{S}_a$, i.e. increasing the a priori uncertainty, yields an increased LWC error and a larger number of DGF implying that the measurements have more weight in the solution. In other words, the better known the a priori profile is, the smaller is the error of the solution and the smaller is the influence of the measurements. If the a priori profile would be the true profile, the measurements would add no information at all. However, in virtually all cases the a priori profile is not the true profile (else there would be no need to perform a retrieval), and the DGF is much lower than the desired resolution of the LWC profile.

3.1. Dependence on measurement vector

We start the analysis by investigating the effect of different measurement combinations on the retrieved LWC error (diagonal elements of $\mathbf{S}$) and on the number of degrees of freedom (trace of $\mathbf{A}$) for the average cloud A (Fig. 4 a,c) and the thick cloud B (Fig. 4 b,d). The different symbols in the diagram represent different a priori uncertainties, which have been varied from $6 \cdot 10^{-4}$ to 7 gm^{-3} (cf. Fig. 3a). The maximum possible number of DGF corresponds to the number of cloud layers on which the LWC is retrieved, i.e. 16 for cloud A and 28 for cloud B. When using the K-band (22–32 GHz) channels only (for cloud A: same curve as in Fig. 3b), there is essentially only one piece of information in

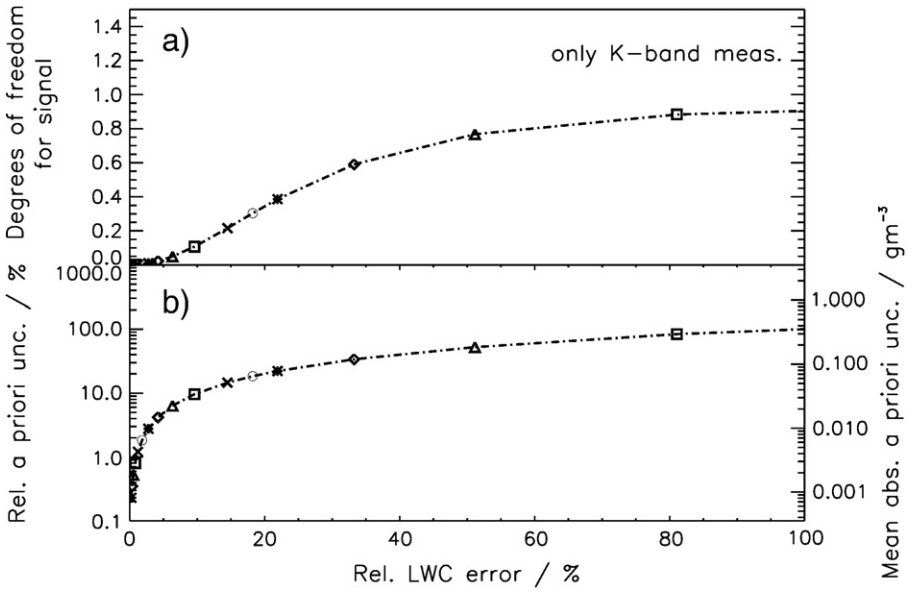

Fig. 3. Degrees of freedom for signal and LWC errors (%) for cloud A assuming different a priori errors (a). The corresponding a priori uncertainties (relative and absolute in gm^{-3}) are shown for reference (b). Different values of the a priori uncertainty are represented by different symbols. The retrieval only includes the MWR brightness temperatures of the K-band.

the measurements, which corresponds to the column integrated LWC, the LWP. Adding the V-band (51–59 GHz), 90, and 150 GHz channels leads to a slightly increased number of DGF for cloud A. Furthermore, this measurement combination reduces the error in the LWC. The maximum information content of the K-band retrieval, i.e. 0.9, is reached for an a priori uncertainty of about 100% corresponding to a LWC error of the same order of magnitude. When adding the other microwave radiometer channels, this value is reached already for a relative error of 10% in the a priori profile. This effect is due to the increased sensitivity of liquid water at 90 and 150 GHz relative to the channels in the K- and V-bands. The TB enhancement of the cloud A on the 90 and 150 GHz TBs is 17 and 19 K, respectively, and only 2–4 K for the K-band and maximum 4 K for the V-band channels (not shown). For the thick cloud (case B), the signal is strong in all channels, namely about 20 K for the K- and V-band and 100 K for the 90 and 150 GHz channels, so that the saturation value of 1 DGF for the K-Band retrieval is reached for a LWC error of 10%. If the V-Band channels and the 90 and 150 GHz frequencies are included, there is a small amount of information on the LWC profile (1.5 DGF). However, this increased information content is reached at a large error in LWC.

Extending this analysis for the inclusion of cloud radar reflectivity data. we start with the simple case that only cloud radar reflectivity (Z) data are used in the retrieval. Recall that we assume an error in Z of 3 dB and, as for the microwave brightness temperatures, that the error is uncorrelated between different radar height bins. In this case, the DGF rapidly increases when the influence of the a priori information is reduced (i.e., when the uncertainty in the a priori profile is increased). The number of DGF is maximal (16 and 28 for cloud A and cloud B, respectively, corresponding to the number or radar bins) for a relative LWC error of 63% in both cases. In this situation, the a priori profile has virtually no effect on the retrieved LWC profile. If the MWR radiometer frequencies are additionally included in the retrieval, the amount of information increases roughly by the number of DGF that are in the MWR observations alone. In Table 1, the DGF associated to a retrieved LWC error of 30% are summarized for the different measurement combinations. A value of 30% is a realistic lower bound for a LWC error using the combination of a cloud radar and microwave radiometer (Löhnert et al., 2001). It is clearly visible that the retrieval including all measurements outperforms the other combinations. The amount of information coming from the measurements increases from about 3% (only K-Band TBs, i.e. 0.5 and 1 of the maximum 16 and 28 DGF, respectively) to 30% (all measurements, i.e. 5 and 8 of the maximum 16 and 28 DGF, respectively). For the thick cloud, the inclusion of the V-band and 90/150 GHz channels only marginally increases the information in the observations compared to the Z-TB_K retrieval.

In order to achieve a relative LWC error of 30%, the a priori uncertainty must be smaller than 34%. Thus for small LWC errors, the retrieved LWC error is of the same order of magnitude as the a priori error itself. However, the spread between a priori and retrieved error and therefore the benefit of the retrieval rapidly increases for a priori errors of about 30% or larger. If the a priori error is about 100%, for example, the retrieval reduces the LWC error to 50%.

3.2. Dependence on measurement error

As mentioned in Section 2, the combined measurement and forward model error in $\mathbf{S}_e$ may be substantially larger. We now want to assess the effect of increasing the measurement error, i.e. the diagonal elements in $\mathbf{S}_e$, on the DGF. For this purpose, we perform an experiment in which we set the TB

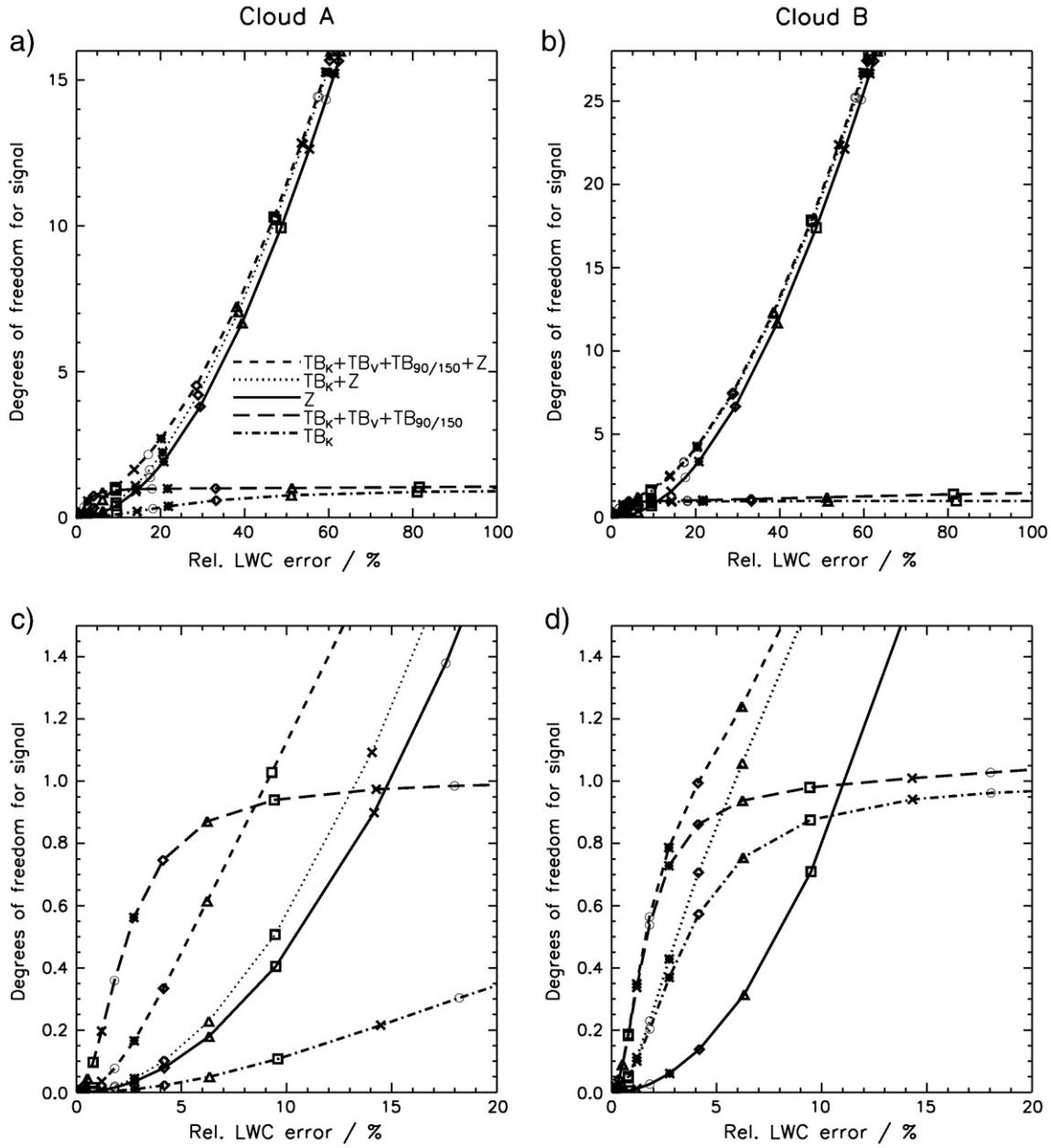

Fig. 4. Degrees of freedom for signal and retrieved LWC errors for cloud A (left panels) and cloud B (right panels) assuming different a priori uncertainties and measurement combinations. The different curves in each panel correspond to different measurement combinations in the retrieval; the seven K-Band channels only (22–32 GHz)(dash-dotted), K- and V-Band channels (51–59 GHz) plus 90 and 150 GHz channels (long dashes), the cloud radar reflectivity measurements only (solid), K-band channels plus cloud radar reflectivities (dotted) and all microwave channels (K-, V-Band, 90, 150) plus cloud radar reflectivities (dashed). Same symbols lying above each other indicate same a priori uncertainties. c) and d) show an image detail of a) and b), respectively.

error to 1 K (Fig. 5a) and leave the Z error unchanged (3 dB) and another one in which the Z error is set to 4 dB and the TB error (0.5 K) is not modified (Fig. 5b). Compared to Fig. 4a, increasing the error in the TB observations reduces the number of DGF for the same relative error in LWC. In other words, the microwave radiometer measurements contribute less to the retrieved LWC profiles as the uncertainty in the radiometer's TB measurements increase. This is especially true for the K-channels (Table 2), since the random error in this spectral band is of the same order of magnitude as the cloud signal in the TBs; the 90 and 150 GHz channels are less affected to small changes in the error in the TB observations because the signals in these channels are stronger. In case of the modified Z errors, the maximum relative error in LWC increases to 88% (not shown) as opposed to the 63% shown in Fig. 4, if the measurements have full weight in the retrieval using reflectivity alone, i.e. if the uncertainty in the a priori profile is large. For the retrieval including all measurements, the maximum LWC error is slightly reduced from 88% to 84%. The increase in the maximum errors reduces the DGF

Table 1
Number of DGF for a retrieved LWC error of 30% assuming different measurement combinations. The maximum number of DGF is 16 for cloud A and 28 for cloud B.

	Cloud A (16 radar bins)	Cloud B (28 radar bins)
TB_K	0.5	1.0
$TB_K + TB_V + TB_{90} + TB_{150}$	0.9	1.1
Z	4.0	6.7
$Z + TB_K$	4.5	8.0
$Z + TB_K + TB_V + TB_{90} + TB_{150}$	5.0	8.0

compared to Fig. 4a (Fig. 5b). In terms of relative changes, the reduction of the DGF is strongest in the retrieval including Z only (about 44%). For small LWC errors, this reduction is

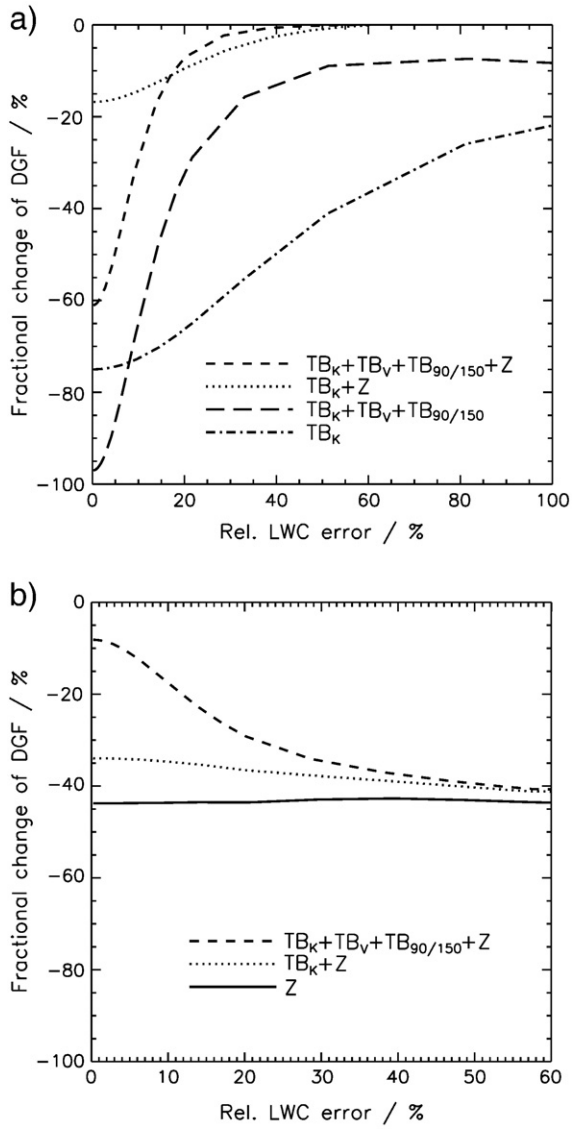

Fig. 5. Percental changes in the DGF compared to results in Fig. 4 a) when assuming larger measurement errors in $\mathbf{S}_e$. (a) Results when setting the TB error to 1 K, leaving the Z error at 3 dB and (b) when setting the Z error to 4 dB, leaving the TB error at 0.5 K.

Table 2
Number of DGF for a retrieved LWC error of 30% assuming different measurement combinations and measurement errors for cloud A.

	$TB_{err} = 0.5$ K, $Z_{err} = 3$ dB	$TB_{err} = 1$ K, $Z_{err} = 3$ dB	$TB_{err} = 0.5$ K, $Z_{err} = 4$ dB
TB_K	0.5	0.2	0.5
$TB_K + TB_V + TB_{90} + TB_{150}$	0.9	0.8	0.9
Z	4.0	4.0	2.2
$Z + TB_K$	4.5	4.2	2.8
$Z + TB_K + TB_V + TB_{90} + TB_{150}$	5.0	4.8	3.1

significantly less pronounced in the retrievals which also encompass the MWR TBs, in particular the measurements at 90 and 150 GHz. For a 30% LWC error, the number of DGF is reduced by about 34% (radar plus all MWR TBs) to 44% (only radar) corresponding to about 1.8 DGF, so that the DGF range between 2.2 (only radar) and 3.1 (radar plus MWR). In other words, only 14 to 19% of the vertical information on the LWC profile comes from the measurement.

3.3. Dependence on correlated measurement and forward model errors

In the previous sections, we have assumed the measurement errors to be uncorrelated and random, and the errors in the forward model to be uncorrelated and random, too. With regard to calibration and forward model errors, this assumption is generally not valid. For the MWR HATPRO, for example, an absolute calibration against an internal hot load target is performed every 5 to 10 min. If the temperature of this internal calibration load is not measured correctly, the MWR brightness temperatures will be systematically too high or too low and the errors of the different channels will be correlated among each other. While such a calibration error can be treated as a systematic error on shorter time scales, i.e. between two calibrations of the instrument, it may be described as a random error on longer timescales, i.e. over several calibration procedures, with significant off-diagonal entries in the covariance matrix $\mathbf{S}_e$.

The effect of such correlated errors on the retrieved error and on the DGF is investigated next. For this purpose, one experiment has been performed with brightness temperature covariances of $(0.2\ \mathrm{K})^2$ and another experiment assuming $(1\ \mathrm{dB})^2$ reflectivity covariances for all corresponding off-diagonal elements in $\mathbf{S}_e$. In general, assuming constant correlations is a rather strong simplification. Nevertheless, this is sufficient for a first qualitative assessment of the influence of correlations. The variances are set to $(0.5\ \mathrm{K})^2$ and $(3\ \mathrm{dB})^2$, respectively. If the measurement errors are correlated, we obtain more information about the measurement, than in the case when the off-diagonal elements are set to zero. Introducing correlated radar reflectivity errors leads to an increased number of DGF and a reduced LWC error calculated for the same a priori errors. For the chosen configuration, up to 0.4 DGF are added, while the relative LWC error is reduced by up to 3%.

Introducing TB covariances of $(0.2\ \mathrm{K})^2$ does not increase the information content of the microwave measurements with regard to the LWC retrieval. Only when very large TB

error correlations of 0.95 and more are introduced, the DGF increases by about 0.6 for small a priori errors.

3.4. Dependence on cloud vertical correlation

In the previous sections, we have assumed that the cloud layers in the a priori profile are uncorrelated, i.e. the off-diagonal components in $\mathbf{S}_a$ are zero. Since the LWC profiles of stratiform clouds are often close to quasi-adiabatic (Korolev et al., 2007), the cloud layers will generally not be independent from each other. In order to assess the effect of cloud vertical correlation on the DGFs and on the retrieved LWC we perform an experiment in which we assume that the correlation of two cloud layers exponentially decreases with their distance to each other (Fig. 6a), such that the covariance of two layers i and j can be written as

$$S_{ij} = \sigma_a^2 exp\left(-0.5\,(i-j)^2 / \beta^2\right) \quad (3)$$

where σ_a^2 is the diagonal entry of $\mathbf{S}_a$. The parameter β is set to 1 and 3, respectively, where the larger value implies a stronger correlation of the cloud layers in the a priori profile. If the cloud layers are correlated and therefore also the errors, the a priori profile has more weight in the retrieval than in the uncorrelated case. The influence of the a priori profile on the solution increases with the correlation. The effect on the relative LWC error and on the pieces of information which come from the measurement is shown in Fig. 6b. Introducing correlation leads to a reduced LWC error, but also to a reduced number of DGF, since we put more confidence in the a priori profile.

3.5. Drizzle case analysis

As mentioned in Sections 1 and 2, Z-LWC relationships are less accurate for clouds including drizzle than for clouds without drizzle. Krasnov and Russchenberg (2002, 2006) have developed a technique which distinguishes light drizzling and heavy drizzling clouds from non-drizzling clouds using radar reflectivity to lidar optical extinction ratio thresholds. In heavy drizzling situations, they found a Z-LWC relationhip with parameters a = 323.59 and b = 1.58. In this case, the forward model error increases to about 5 dB. Remember, that in non-drizzling situations the error has been estimated to be about 1.5 to 3 dB.

We repeat the analysis for cloud A and B assuming that we are dealing with heavy drizzling clouds. Since we apply a different forward model, i.e. the formulation for heavy drizzling clouds by Krasnov and Russchenberg (2002, 2006), with different error characteristics, the Jacobian $\mathbf{K}$ and the elements in $\mathbf{S}_e$ have to be adapted. The diagonal elements of $\mathbf{S}_e$ are now the sum of the square of the measurement error (3 dB) and the square of the forward model error (5 dB) and are therefore 34 dB^2.

Compared to Fig. 4, the trade-off between the relative error in LWC and the DGF is qualitatively similar (not shown). However, the maximum LWC error, i.e. the error associated with the maximum number of DGF, is 96% for the retrieval employing the radar reflectivities only. This means that, without a priori information and fully relying on the Z-LWC relationship, the error of the retrieved LWC is almost 100%.

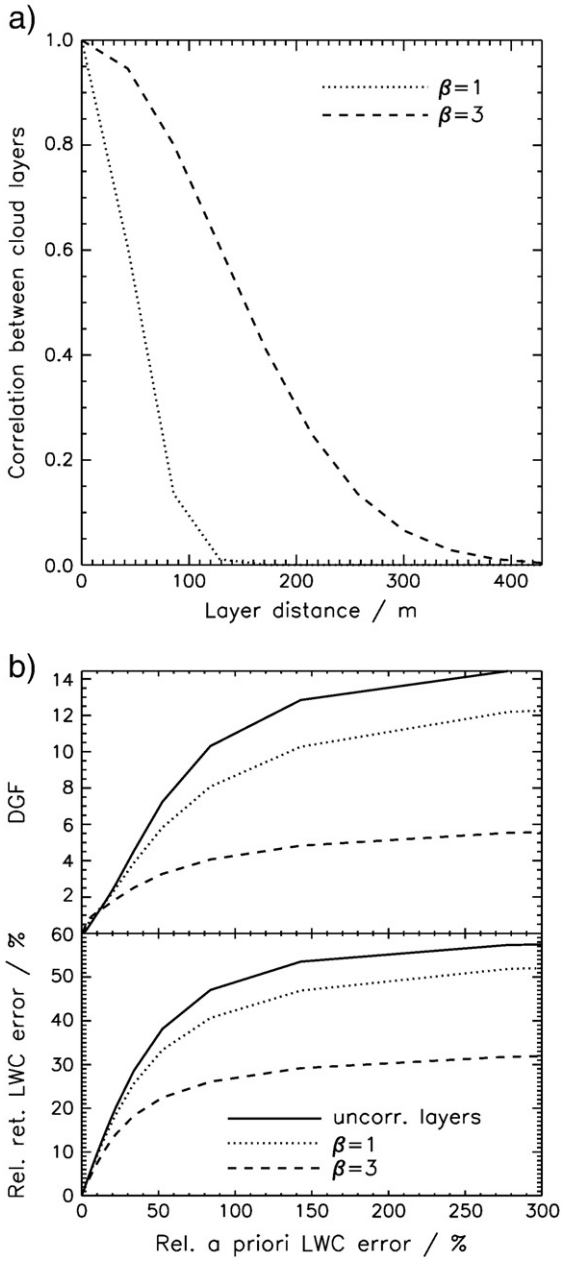

Fig. 6. Sensitivity of the DGF to non-zero, off-diagonal elements in $\mathbf{S}_a$. (a) Correlation between two layers within a cloud as a function of their distance to each other according to Eq. (3). (b) Relative LWC error (bottom) and degrees of freedom for signal (top) as a function of the a priori LWC error for cloud A using all microwave channels (K-, V-Band, 90, 150) and cloud radar reflectivities. The three curves in each panel of b) represent different values of β in $\mathbf{S}_a$. No correlation of cloud layers, i.e. zero off-diagonal elements ($\beta = 0$, solid), correlation of cloud layers corresponding to curves in a) ($\beta = 1$, dotted; $\beta = 3$, dashed).

For a 30% error in the retrieved LWC, a priori information has to be included, whose accuracy must be at least 32%. However, in this case, only 1.9 DGF (cloud A) and 3.3 DGF (cloud B) are in the measurements. In other words, 88% of the vertical information comes from the a priori profile. When

adding the MWR measurements, this is at least reduced to 81%, since the MWR TBs add about 1 DGF.

3.6. Impact on radiative fluxes and heating rates

As mentioned in Section 1, accurate LWC profiles are essential for radiative transfer applications and for the assessment of the effect of clouds on broadband fluxes and heating rates. In order to get an idea of the sensitivity of fluxes and heating rates with respect to LWC errors, we assumed a LWC uncertainty of 30% and applied the LWC profiles to a broadband radiative transfer model, namely the Rapid Radiative Transfer Model (RRTMG) of the Atmospheric and Environmental Research (AER), Inc. (Mlawer et al., 1997; Clough et al., 2005). The RRTMG is a correlated-k model using the gaseous absorption coefficients directly from the line-by-line radiative transfer model (LBLRTM) of the AER, Inc. Fluxes and heating rates are calculated over 14 contiguous bands in the shortwave and 16 in the longwave regime. For multiple scattering, a two-stream algorithm is used (Oreopoulos and Barker, 1999).

Since the droplet effective radius is also needed as an input parameter in the RRTMG, we calculated the effective radius according to Frisch et al. (1995) with an assumed total number concentration of 288 cm^{-3} and a lognormal size distribution width of 0.38, which both represent mean values of continental clouds (Miles et al., 2000). Temporally interpolated radiosonde data were applied to derive the required thermodynamic profiles. The solar surface albedo was set to 0.2 and the cosine of the solar zenith angle to 0.7, leading to an incident top of atmosphere solar flux of about 945 Wm^{-2}. The radiative transfer calculations have been performed using the vertical resolution of the cloud radar, i.e. about 43 m.

First, fluxes and heating rates have been calculated using the original LWC profiles shown in Fig. 1. Then, the LWC has been varied by 30% resulting in LWP variations of 27.8 gm^{-2} and 206.5 gm^{-2} for cloud A and B, respectively. The calculated shortwave (SW) and longwave (LW) cloud radiative effect (CRE) at the surface, which is defined as the difference of the cloudy and clear sky net surface fluxes, is shown in Table 3. SW fluxes are most sensitive to variations in the LWP, when the LWP is small (cf. Fig. 5 in Sengupta et al., 2003, Turner et al. 2007b). Thus, a LWC uncertainty of 30% leads to a larger uncertainty in the SW CRE for cloud A than for cloud B, since the LWP of cloud A (92.7 gm^{-2}) is considerably smaller than the LWP of cloud B (688.4 gm^{-2}). Reducing the LWC leads to a reduced SW cooling by 46.9 Wm^{-2} (cloud A) and 19.9 Wm^{-2} (cloud B), while enlarging the LWC enhances the SW cooling by 30.4 Wm^{-2} (cloud A) and 11.1 Wm^{-2} (cloud B). The variations in LWC have only a small effect on the cloud induced LW warming at the surface with differences of up to 0.5 Wm^{-2} because the clouds are opaque in the infrared and the LW warming at the surface is more sensitive to changes in cloud base height.

Table 3
Shortwave and longwave cloud radiative effect (CRE) at the surface (Wm^{-2}) for cloud A and B assuming an LWC error of 30%. The cloud radiative effect is defined as the difference between the cloudy and clear sky net fluxes. The corresponding values of the LWP (gm^{-2}) are also shown.

	Cloud A			Cloud B		
	LWP (gm^{-2})	SW CRE (Wm^{-2})	LW CRE (Wm^{-2})	LWP (gm^{-2})	SW CRE (Wm^{-2})	LW CRE (Wm^{-2})
Orig. LWP	92.7	−422.3	68.1	688.4	−551.4	80.5
−30%	64.9	−375.4	67.8	481.9	−531.5	80.3
30%	120.5	−452.7	68.3	894.9	−562.5	80.7

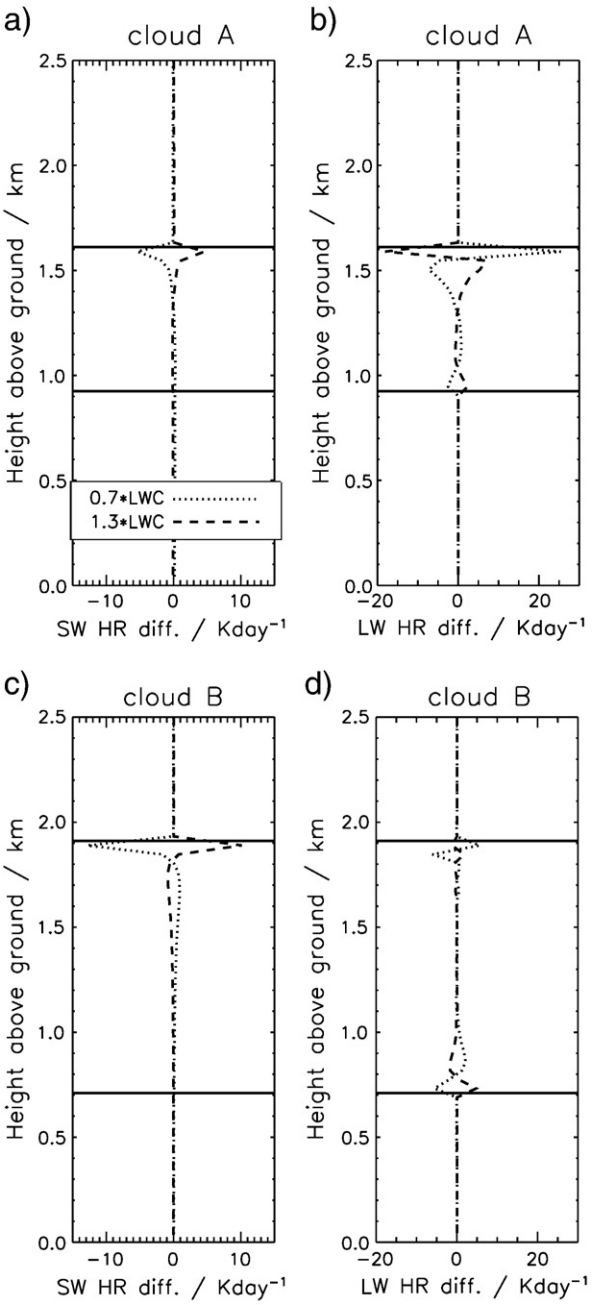

Fig. 7. Sensitivity tests of SW and LW heating rates with respect to LWC variations of 30%. Changes are relative to the HR of the original LWC profiles. (a) and (b), SW and LW HR differences (K day^{-1}) for cloud A; (c) and (d) SW and LW HR differences for cloud B. The cloud boundaries are indicated by horizontal solid lines.

The effect on the LW heating rates, especially at the cloud boundaries can be significant. Fig. 7 shows the differences of the heating rates compared to the results with the original LWC profiles. LW cooling at cloud top is about −137 and −265 K day^{-1} for clouds A and B, respectively. LW warming in the lower cloud levels is about 10 and 23 K day^{-1}. For cloud A, a reduced LWC leads to a reduced cooling at cloud top by 18% (25 K day^{-1}) but also to a reduced warming at cloud base by 30% (3 K/day^{-1}). Increasing the LWC leads to an opposite effect (stronger cooling at cloud top, stronger warming at cloud base). The LW heating rate differences of the thicker cloud are less pronounced, especially with respect to the large cloud top cooling of −265 K day^{-1}.

For the SW heating rates, the differences are visible in the uppermost cloud levels. Increasing the LWC by 30% results in an increased absorption of SW radiation in these levels and increases the SW heating rate by about 4 K day^{-1} (cloud A) and 9 K day^{-1} (cloud B), which corresponds to a relative increase of about 16% and 12%, respectively. Reducing the LWC reduces the SW heating rate by essentially the same amounts.

It has been shown that variations in the LWC profiles can strongly affect the surface energy balance and the atmospheric heating rates. Since the vertical redistribution of energy by clouds has an important impact on the atmospheric dynamics and the hydrological cycle (Stephens, 2005), uncertainties in LWC and therefore corresponding uncertainties in heating rates will have an impact on related physical processes, too. However, to assess the overall impact on other NWP model variables, sensitivity studies have to be performed in the whole model framework including all physical components.

4. Summary and outlook

In this study, we assessed the influence of a priori, measurement and forward model errors on the information content in the measurements with respect to the LWC retrieval and on the retrieved LWC errors. If the a priori uncertainties are small compared to the measurement and forward model errors, the a priori profile dominates the solution; if they are large, the LWC profile information comes primarily from the measurements. The DGF and the retrieved LWC errors are also sensitive to the measurements themselves which are included in the retrieval, i.e. MWR TBs, radar reflectivities or a combination of both.

By means of two realistic LWC profiles, we have demonstrated that sensor synergy, i.e. the combination of cloud radar reflectivity and MWR brightness temperature observations, outperforms other retrievals using data from one instrument alone. More precisely, MWR measurements can increase the information content compared to a retrieval using radar reflectivities alone and add about 1 degree of freedom for signal corresponding to the information of the LWP. Thus, the results of Crewell et al. (2009) are confirmed in that the zenith MWR measurements alone do not contain enough information about the vertical profile of LWC. Radar reflectivity measurements alone do include information on the vertical distribution of liquid water content. However, for the two non-drizzling cloud cases, the error in the derived LWC is 63% assuming that the a priori profile is unknown and the measurement error is 3 dB. This error is reduced by a few percent, if the individual measurement errors are correlated.

In drizzle situations, Z-LWC-relationships are less reliable and retrieved LWC errors are 100% or larger. LWC profiles with such large errors are not desirable, as the uncertainty in the radiative fluxes that arise from the uncertainties in LWC can be significant. In order to diminish the LWC errors, appropriate a priori information has to be included. By means of the two cloud cases, we demonstrated that for realistic measurement errors of 0.5 K and 3 dB for MWR brightness temperatures and radar reflectivities, respectively, the uncertainty of the a priori profile must be smaller than 100% to achieve a relative LWC error of 50% in non-drizzling cases. While for small a priori uncertainties the retrieved LWC error is of the same order of magnitude as the a priori error itself, the spread between a priori and retrieved error and therefore the benefit of the retrieval rapidly increases for a priori errors of about 30% or larger.

The importance of the a priori profile has been emphasized with regard to a drizzle situation, when the Z-LWC relationship is less accurate. In order to achieve a 50% (30%) LWC error in the drizzling cloud case, the a priori uncertainty must be smaller than 65% (32%).

If the information content in the observation is low because of large measurement or forward model errors, accurate a priori information on the LWC profile is required to keep the error of the solution small. However, the accuracy of the a priori profile (in the IPT the accuracy of the cloud model by Karstens et al. (1994)), is not well known and it is questionable if a 32% a priori uncertainty is a realistic value. Furthermore, the correlation of the cloud layers, and therefore the off-diagonal elements in $\mathbf{S}_a$, are relatively unknown and better statistics are needed in this respect to describe the errors accurately. Furthermore, it is likely that the a priori profile, and especially the correlation between different levels in the a priori profile, is very dependent on the synoptic and mesoscale conditions that are driving the cloud formation/evolution. Therefore, not only the accuracy of the measurements and the forward models must be improved, but also the knowledge of the a priori profile. In this respect, more in situ data are needed which span the wide range of atmospheric conditions and corresponding LWC profiles. This information could be gained, for example, from unmanned aerial vehicles (UAVs), which are equipped with a LWC sensor, e.g. a forward spectral scattering or a Nevzorov probe. From such measurements, more accurate a priori LWC profiles and realistic layer to layer covariances could be derived. In this context, the RACORO experiment of the ARM Aerial Vehicle Program is promising, which took place from January to June 2009 in the vicinity of the ARM Southern Great Plains measurement site (http://acrf-campaign.arm.gov/racoro). For the first time, a long-term aircraft campaign was undertaken for the systematic in situ sampling of boundary-layer water cloud properties.

The applied formalism allows for the inclusion of additional measurements or instruments to further constrain the solution. Since cloud radars are insensitive to the smallest droplets located near the bottoms of cloud, lidar measurements, which are sensitive to higher concentration of smaller particles, can provide valuable information for these heights. In this context, Raman lidar measurements can be used to

derive vertical profiles of LWC (Whiteman and Melfi, 1999). The drizzling clouds (Section 3.4) can be identified and mitigated by using information of a dual-wavelength radar. Hogan et al. (2005) showed that in boundary layer clouds, accurate LWC profiles can be retrieved from 35 GHz and 94 GHz cloud radar measurements, if the droplets scatter in the Rayleigh regime at both frequencies. The advantage of this technique is that no assumptions on the droplet size distribution have to be made. Spectral infrared measurements could also improve the solution in cases where LWP is low ($<50\ \mathrm{gm}^{-2}$) since they are very sensitive to changes in liquid water in this regime (Turner 2007). As a first step, Löhnert et al. (2009) successfully combined MWR measurements with information of an infrared spectrometer in the framework of the IPT to derive profiles of temperature and humidity. As a next step, it is planned to extend this retrieval to a combined scheme for thermodynamic and cloud properties, and to incorporate cloud radar measurements to aid in the retrieval of cloud microphysical properties.

Retrievals as described in this paper have a large potential since the strengths of individual measurement systems are combined yielding a comprehensive characterization of the atmospheric state.

Acknowledgements

The IPT retrieval used data obtained by the Atmospheric Radiation Measurement (ARM) Program sponsored by the U.S. Department of Energy, Office of Science, Office of Biological and Environmental Research, Climate and Environmental Sciences Division. We would like to thank Ewan O'Connor who provided the Cloudnet Target Categorization product included in the IPT and Wenchieh Yen who helped with the radiative transfer calculations.

References

Atlas, D., 1954. The estimation of cloud parameters by radar. J. Meteor. 11, 309–317.

Clough, S.A., Shephard, M.W., Mlawer, E.J., Delamere, J.S., Iacono, M.J., Cady-Pareira, K., Boukabara, S., Brown, P.D., 2005. Atmospheric radiative transfer modeling: A summary of the AER codes. J. Quant. Spectrosc. Radiative Trans. 91, 233–244.

Crewell, S., Löhnert, U., 2003. Accuraccy of cloud liquid water path from ground-based microwave radiometry. Part II. Sensor accuracy and synergy. Radio Sci. 38 (3). doi:10.1029/2002RS002634.

Crewell, S., Ebell, K., Löhnert, U., Turner, D., 2009. Can liquid water profiles be retrieved from passive microwave zenith observations? Geophys. Res. Lett. 36. doi:10.1029/2008GL036934.

Fox, N.I., Illingworth, A.J., 1997. The retrieval of stratocumulus cloud properties by ground-based cloud radar. J. Appl. Meteor. 36, 485–492.

Frisch, A., Fairall, C., Snider, J., 1995. Measurement of stratus cloud and drizzle parameters in ASTEX with a Kα-Band doppler radar and a microwave radiometer. J. Atmos. Sci. 52, 2788–2799.

Frisch, A.S., Feingold, G., Fairall, C.W., Uttal, T., Snider, J.B., 1998. On cloud radar and microwave measurements of stratus cloud liquid water profiles. J. Geophys. Res. 103, 23195–23197.

Handwerker, J., Miller, M.A., 2008. Intercomparison of measurements obtained by vertically pointing collocated 95 GHz and 35.5 GHz cloud radars. Proc. Fifth European Conference on Radar in Meteorology and Hydrology, Helsinki, Finland, Finish Meteorological Institute, P5.3. Available online at http://erad2008.fmi.fi/proceedings/extended/erad2008-0124-extended.pdf.

Hogan, R.J., Gaussiat, N., Illingworth, A.J., 2005. Stratocumulus liquid water content from dual-wavelength radar. J. Atmos. Oceanic Technol. 22, 1207–1218.

Illingworth, A.J., Hogan, R.J., O'Connor, E.J., Bounoil, D., Brooks, M.E., Delanoë, J., Donovan, P., Eastment, J.D., Gaussiat, N., Goddard, J.W.F., Haeffelin, M., Klein, H., Baltink, H.K., Krasnov, O.A., Pelon, J., Piriou, J.-M., Protat, A., Russchenberg, H.W.J., Seifert, A., Tompkins, A.M., van Zadelhoff, G.-J., Vinit, F., Willén, U., Wilson, D.R., Wrench, C.L., 2007. CLOUDNET continous evaluation of cloud profiles in seven operational models using ground-based observations. Bull. Amer. Meteor. Soc. 88 (6), 883–898.

Karstens, U., Simmer, C., Ruprecht, E., 1994. Remote sensing of cloud liquid water. Meteor. Atmos. Phys. 54, 157–171.

Khain, A., Pinsky, M., Magaritz, L., Krasnov, O., Russchenberg, H., 2008. Combined observational and model investigations of the Z-LWC relationship in stratocumulus clouds. J. Appl. Meteor. Clim. 47, 591–606.

Korolev, A.V., Isaac, G.A., Strapp, J.W., Cober, S.G., Barker, H.W., 2007. In situ measurements of liquid water content profiles in midlatitude stratiform clouds. Q. J. R. Meteorol. Soc. 133, 1693–1699.

Krasnov, O.A., Russchenberg, H.W.J., 2002. The relation between the radar to lidar ratio and the effective radius of droplets in water clouds: an analysis of statistical models and observed drop size distributions. Preprints, 11th Conf. on Cloud Physics, Ogden, Utah. Amer. Meteor. Soc, p. P1.7.

Krasnov, O.A., Russchenberg, H.W.J., 2006. A synergetic radar-lidar technique for the LWC retrieval in water clouds. Preprints, Seventh Int. Symp. on Tropospheric Profiling: Needs and Techniques, Boulder, CO.

Liebe, H.J., Hufford, G.A., Manabe, T., 1991. A model for the complex permittivity of water at frequencies below 1 THz. Int. J. Infrared & Millimeter Waves 12 (7). doi:10.1007/BF01008897.

Liebe, H.J., Hufford, G.A., Cotton, M.G., 1993. Propagation modeling of moist air and suspended water/ice particles at frequencies below 1000 GHz. Atmospheric Propagation Effects through Natural and Man-Made Obscurants for Visible through MM-Wave Radiation, AGARD-CP-542, pp. 3.1–3.10.

Löhnert, U., Crewell, S., Simmer, C., Macke, A., 2001. Profiling cloud liquid water by combining active and passive microwave measurements with cloud model statistics. J. Atmos. Oceanic Technol. 18, 1354–1366.

Löhnert, U., Crewell, S., Simmer, C., 2004. An integrated approach towards retrieving physically consistent profiles of temperature, humidity and cloud liquid water. J. Appl. Meteor. 43, 1295–1307.

Löhnert, U., Crewell, S., Krasnov, O., O'Connor, E., Russchenberg, H., 2008. Advances in continuously profiling the thermodynamic state of the boundary layer: integration of measurements and methods. J. Atmos. Oceanic Technol. 25, 1251–1266.

Löhnert, U., Turner, D.D., Crewell, S., 2009. Ground-based temperature and humidity profiling using spectral infrared and microwave observations: Part 1. Retrieval performance in clear sky conditions. J. Appl. Meteor. Clim. 5, 1017–1032.

Mace, G.G., et al., 2006a. Cloud radiative forcing at the atmospheric radiation measurement program climate research facility: 1. Technique, validation, and comparison to satellite derived diagnostic quantities. J. Geophys. Res. 111, D11S90. doi:10.1029/2005JD005921.

Mace, G.G., Benson, S., Kato, S., 2006b. Cloud radiative forcing at the atmospheric radiation measurement program climate research facility: 2. Vertical redistribution of radiant energy by clouds. J. Geophys. Res. 111, D11S91. doi:10.1029/2005JD005922.

Mace, G.G., Benson, S., 2008. The vertical structure of cloud occurrence and radiative forcing at the SGP ARM site as revealed by 8 years of continuous data. J. Clim. 21, 2591–2610.

Mather, J., McFarlane, S., Miller, M., Johnson, K., 2007. Cloud properties and associated radiative heating rates in the tropical western Pacific. J. of Geophys. Res. 112, D05201. doi:10.1029/2006JD007555.

Mattioli, V., Basili, P., Bonafoni, S., Ciotti, P., Pulvirenti, L., Pierdicca, N., Marzano, F.S., Consalvi, F., Fionda, E., Westwater, E.R., 2006. Cloud liquid models for propagation studies: Evaluation and refinements. Proc. 'EuCAP 2006' , Nice, France, 6–10 November 2006 (ESA SP-626, October 2006).

McFarlane, S., Mather, J., Ackerman, T., Liuand, Z., 2008. Effect of clouds on the calculated vertical distribution of shortwave absorption in the tropics. J. Geophys. Res. 113, D18203. doi:10.1029/2008JD009791.

Miles, N., Verlinde, J., Clothiaux, E., 2000. Cloud droplet size distributions in low-level stratiform clouds. J. Atmos. Sci. 57, 295–311.

Mlawer, E.J., Taubman, S.J., Brown, P.D., Iacono, M.J., Clough, S.A., 1997. Radiative transfer for inhomogeneous atmospheres: RRTM, a validated correlated-k model for the long wave. J. Geophys. Res. 102, 16,663–16,682.

Oreopoulos, L., Barker, H.W., 1999. Accounting for subgrid-scale cloud variability in a multi-layer 1-D solar radiative transfer algorithm. Quart. J. Roy. Meteor. Soc. 125, 301–330.

Rodgers, C.D., 2000. Inverse methods for atmospheric sounding: Theory and practice. World Scientific. 238 pp.

Rose, T., Crewell, S., Löhnert, U., Simmer, C., 2005. A network suitable microwave radiometer for operational monitoring of the cloudy atmosphere. Atmos. Res. 75, 183–200.

Rosenkranz, P.W., 1998. Water vapor microwave continuum absorption: a comparison of measurements and models. Radio Sci. 33, 919–928.

Salonen, E., Uppala, S., 1991. New prediction method of cloud attenuation. Electronic Newsletter 27 (No.12), 1106–1110.
Sauvageot, H., Omar, J., 1987. Radar reflectivity of cumulus clouds. J. Atmos. Ocean. Tech. 4, 264–272.
Sengupta, M., Clothiaux, E., Ackerman, T., Kato, S., Min, Q., 2003. Importance of accurate liquid water path for estimation of solar radiation in warm boundary layer clouds: an observational study. J. Clim. 16, 2997–3009.
Stephens, G.L., 2005. Cloud feedbacks in the climate system: a critical review. J. Atmos. Sci. 18, 237–273.
Turner, D.D., 2007. Improved ground-based liquid water path retrievals using a combined infrared and microwave approach. J. Geophys. Res. 112, D15204. doi:10.1029/2007JD008530.
Turner, D.D., Clough, S.A., Liljegren, J.C., Clothiaux, E.E., Cady-Pereira, K.E., Gaustad, K.L., 2007a. Retrieving liquid water path and precipitable water vapor from the atmospheric radiation measurement (ARM) microwave radiometers. IEEE Trans. Geosci. Remote Sens. 45 (11), 3680–3690.
Turner, D.D., et al., 2007b. Thin liquid water clouds: their importance and our challenge. Bull. Amer. Meteor. Soc. 88, 177–190.
Turner, D.D., Loehnert, U., Cadeddu, M., Crewell, S., Vogelmann, A., 2009. Modifications to the water vapor continuum in the microwave suggested by ground-based 150 GHz observations. IEEE Trans. Geosci. Remote Sens. 47, 3326–3337. doi:10.1109/TGRS.2009.202262.
Wang, J., Rossow, W.B., 1998. Effects of cloud vertical structure on atmospheric circulation in the GISS GCM. J. Clim. 12, 3010–3029.
Wang, Z., Sassen, K., 2001. Cloud type and macrophysical property retrieval using multiple remote sensors. J. Appl. Meteor. 40, 1665–1682.
Warner, J., 1955. The water content of cumuliform clouds. Tellus 7, 449–457.
Westwater, E., 1978. The accuracy of water vapor and cloud liquid determination by dual-frequency ground-based microwave radiometry. Radio Sci. 13, 667–685.
Whiteman, D.N., Melfi, S.H., 1999. Cloud liquid water, mean droplet radius, and number denisity measurements using a Raman lidar. J. Geophys. Res. 104 (D24), 31,411–31,419.
Webpage of RACORO experiment: http://acrf-campaign.arm.gov/racoro. Last accessed on 7 May 2010.